Open Ceramics 5 (2021) 100076

Contents lists available at ScienceDirect

Open Ceramics

journal homepage: www.editorialmanager.com/oceram

Spark plasma sintering of dense alumina ceramics from industrial waste scraps

Milan Vukšić [a,*], Irena Žmak [a], Lidija Ćurković [a], Andraž Kocjan [b]

[a] Faculty of Mechanical Engineering and Naval Architecture, University of Zagreb, Ivana Lučića 5, 10000, Zagreb, Croatia
[b] Department for Nanostructured Materials, Jožef Stefan Institute, Jamova cesta 39, 1000, Ljubljana, Slovenia

ARTICLE INFO

Keywords:
Circular economy
Sustainability
Ceramics
Spark plasma sintering
Alumina

ABSTRACT

The implementation of environmentally-friendly manufacturing, which include the reuse and recycling of materials is nowadays crucial in order to meet the circular economy approach. The present study shows the possibility of recycling waste alumina scraps obtained after the green machining step during the manufacturing process of alumina ceramics as a broken ware, which contained small amounts (≤5 wt.% in total) of sintering additives in the form of organic binders and MgO. Dense alumina samples containing various amounts of waste alumina powder (0–100 wt.%) were produced by spark plasma sintering (SPS) at sintering temperature of 1450 °C, dwell time of 5 min at a 50 MPa of uniaxial pressure. The influence of waste alumina content on microstructure, hardness, and fracture toughness was investigated to determine the possibility of recycling broken ware.

1. Introduction

The circular economy (CE) concept is focused on stimulating a sustainable approach by promoting the use of recycled materials as a substitute for primary resources [1–3]. Ellen MacArthur Foundation has stated in their report [4] that primary resources made between 40% and 60% of main manufacturing costs. The transformation of generated waste into secondary raw materials leads to cost reductions in the manufacturing processes, boost revenue from waste in the secondary raw market, and consequently reduce the resource dependency [5]. In order to reduce waste generation and achieve a sustainable economy, the new government strategies [6] concerning CE were implemented while numerous studies of various industry sectors were reported [7–9].

The ceramic industry produces different types of solid waste pollutants such as scraps from machining, waste moulds, for example. Moreover, ceramic manufacturing companies can gain considerable financial benefits by recycling the waste as secondary raw material. The usage of generated solid waste in the traditional ceramics industry was mainly reported for floor tile [10], and sanitaryware production [11]. Considering advanced ceramics production, the possibility of reusing 3Y-TZP ceramic waste in the processing of dental ceramics was recently reported [12,13]. The CAD/CAM machining process, where oversize milling of the pre-sintered zirconia blocks is performed, can generate up to 80% waste 3Y-TZP powder scrapes of the initial block mass [14].

Alumina is another major engineering ceramic material processed in big quantities worldwide. It is one of the most important oxide ceramic engineering materials, which has been widely used in many applications because of its convenient properties such as high strength and hardness, thermal stability, wear resistance, and chemical stability [15]. Some studies related to waste alumina recycling in road construction [16] and concrete production process [17,18] were reported, but only a few of the available studies reported recycling solid waste within a ceramic manufacturing process [19–21]. During industrial manufacturing of alumina ceramics, different kinds of process losses in terms of scraps are generated. The scraps can be reused and recycled within the manufacturing process if they fulfil the product specifications such as dimensional tolerance, density, strength, hardness, durability, and refractoriness; otherwise, they are considered as waste and disposed to external disposal facilities [22].

The desired product specifications of alumina ceramics can be met by implementing different sintering techniques. In this way, the desired impact can be made to affect the finer grain size, porosity, and density after the sintering process. One of the novel sintering techniques is the Spark Plasma Sintering (SPS) which attracts attention as a highly promising technique for materials sintering [15,23,24]. The reduced sintering time due to short holding times, high heating rates (up to 500 °C/min) are the main advantages of SPS compared to conventional sintering [25–27]. SPS, thus, has a great potential for obtaining denser and

* Corresponding author.
E-mail address: milan.vuksic@fsb.hr (M. Vukšić).

https://doi.org/10.1016/j.oceram.2021.100076
Received 28 October 2020; Received in revised form 15 February 2021; Accepted 17 February 2021
Available online 23 February 2021

Table 1
Chemical composition of pure (C 90 LSB) and waste alumina powder.

Powder	Component	MgO	Fe_2O_3	SiO_2	Na_2O	CaO	Al_2O_3
C 90 LSB	wt.%	0.066	0.015	0.02	0.05	0.013	99.836
Waste[a]	wt.%	0.1	0.02	0.02	0.08	0.03	99.7

[a] Used in the first cycle of manufacturing.

finer microstructures due to the ablity to exert densification at limited grain growth [28–30]. The utilization of the SPS technique for sintering commercially available alumina was reported previously [31–34]. Conducted studies suggested different optimal sintering conditions depending on powder characteristics and sample's green density, which resulted in fully dense samples with limited grain growth. As a consequence of microstructure refinement by MgO addition, enhanced mechanical properties such as the significant increase of hardness values and slight improvement of fracture toughness were reported [35,36].

The main objective of this study is to determine the possibility of reusing waste alumina powder as a secondary raw material to produce high-quality technical ceramics via SPS technique. For that purpose, wide ranges of waste alumina powder, which contain up to 5 wt.% of the organic binder and 0.1 wt.% MgO, were mixed with cheap and commercially available alumina powder. The effect of waste alumina content on mechanical properties was compared to the available literature data. The possibility of reusing powdered scraps (waste alumina) would bring significant improvements in ceramic manufacturing by decreasing waste production, energy consumption, and ultimately lead to a sustainable and cost-effective process.

2. Experimental procedure

2.1. Starting alumina powders

The waste alumina powder used in this study was generated during the ceramic production process. In the first step, a spray-dried thermally reactive alumina powder, which contains up to 5 wt.% of the organic binder was pressed at high pressure into a pre-designed mould to form a raw shape. After the pressing, the ceramic compact was subjected to the green machining as closely as possible to desired final dimensions. The green machining is far more economically favourable than post-machining after the sintering process. The broken ware (waste alumina powdered scraps) generated during this forming step was collected by industrial dust sucking machine into bags for further storage.

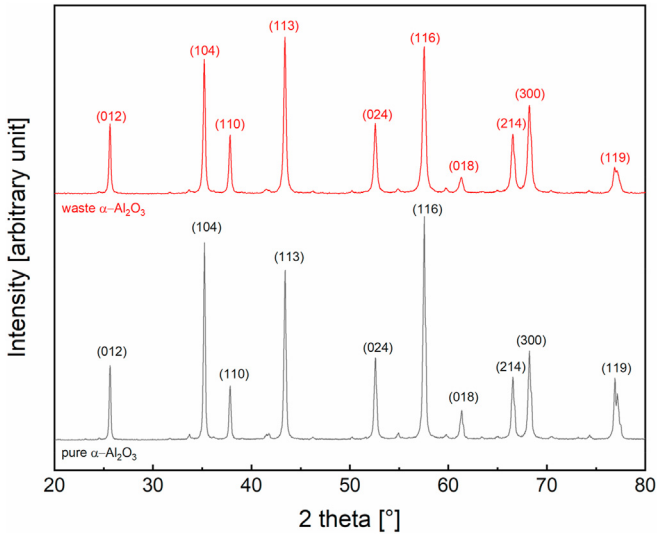

Fig. 1. The XRD patterns of pure and waste alumina powder, which were collected as absolute intensity versus 2 theta in the range from 20 till 80°.

Commercially available high-purity 99.5% alumina powder (C 90 LSB Alumina, Alcan Chemicals, USA), was used as the primary material. In Table 1 the chemical composition of used alumina powders is shown.

The particle size distributions (PSD) of both powders and their mixtures were determined by the laser diffraction method (Horiba LA-920, Kyoto, Japan). Prior to the measurements, the aqueous dispersions containing pure and waste alumina powders, and their respective mixtures were made using the Dolapix® (Zschimmer & Schwarz GmbH Co., Germany) as a dispersant agent, followed by intensive mixing and an ultrasonic horn design treatment of the aqueous dispersions. The specific surface area was determined by the Brunauer-Emmett-Teller (BET) nitrogen adsorption analyser (Quantachrome Nova 2000e, Anton Paar QuantaTec Inc., Austria). XRD analyses (AXS D4 Endeavor, Bruker AXS GmbH, Germany) were conducted on as received starting alumina powders for secondary phases or impurities. The measurement conditions were as follows: CuKα radiation at ambient temperature, the 2θ range from 20° to 80°, step size 0.04, and acquisition time per a channel of 3 s.

2.2. Powder processing and sintering

The waste and commercial alumina powders were sintered as received while various mixtures of Al_2O_3 (commercial powder) Al_2O_3 (waste powder) were prepared using ethanol as liquid media via ball milling (PM100, Retsch GmbH, Germany). The milling process was conducted in a steel container with interior alumina coating and alumina balls at 300 rpm for 2 h. The prepared suspensions were dried to obtain powder form. The mixtures of alumina powders ranging from 20 to 80 wt.%, commercial, and waste alumina were sintered by SPS (Dr. Sinter 3000, SPS Syntex Inc., Japan). The weight amount of 1.96 g for each sintering was placed into a graphite die with an inner diameter of 16 mm. In order to secure easy removal of the sample after the sintering, a thin graphitic sheet was positioned between the powder and the die body. Also, the thermal insulation of the die was achieved by using graphitic foam. After placing the die into the SPS chamber and focusing an optic pyrometer on the die to measure and control the sintering temperature, the vacuum pump was activated to achieve chamber pressure which was less than 30 Pa. The common sintering conditions for all sintered samples were a heating rate of 100 °C/min and a cooling rate of 200 °C/min. Also, the uniaxial pressure was programmed to start pressurizing the sample around 600 °C and achieve the desired pressure around 1000 °C. The achieved pressure was maintained the entire dwell time and gradually removed during 1 min. The obtained samples were shaped as a disk with 16 mm diameter and approximately 2 mm of thickness.

2.3. Microstructural and mechanical characterization

Before density measurements, the graphitic sheet was removed from the sample. The density was first roughly estimated by measuring dimensions and the weight of the samples. The more accurate density measurements were performed by the Archimedes method in distillate water using a density meter (JP703C, Mettler-Toledo GmbH, Switzerland). The calculation of density was done according to the rule of mixtures and compared with the reported [37] alumina theoretical density of 3.987 g/cm^3 in order to obtain the relative density of sintered alumina samples. The images of the thermally etched sample surface and fracture surface, metallized with gold, were obtained by scanning electron microscopy (FEI, HeliosNanolab 650, the United States). Samples were previously prepared on Struers® machine by grinding down their surface on diamond plates (MD-Piano 220, followed by MD-Piano 1200 and MD-Largo) and polishing down on a diamond plate (MD-Dac) with additions of 9 μm diamond paste and finally 3 μm. After the ceramographic procedure, the samples were subjected to thermal etching in an electric furnace (Nabertherm GmbH, Bremen, Germany). The sintering stage was consisted of 10 °C/min heating rate until 1400 °C with a dwell time of 30 min to induce the etching of sample surface for quantification

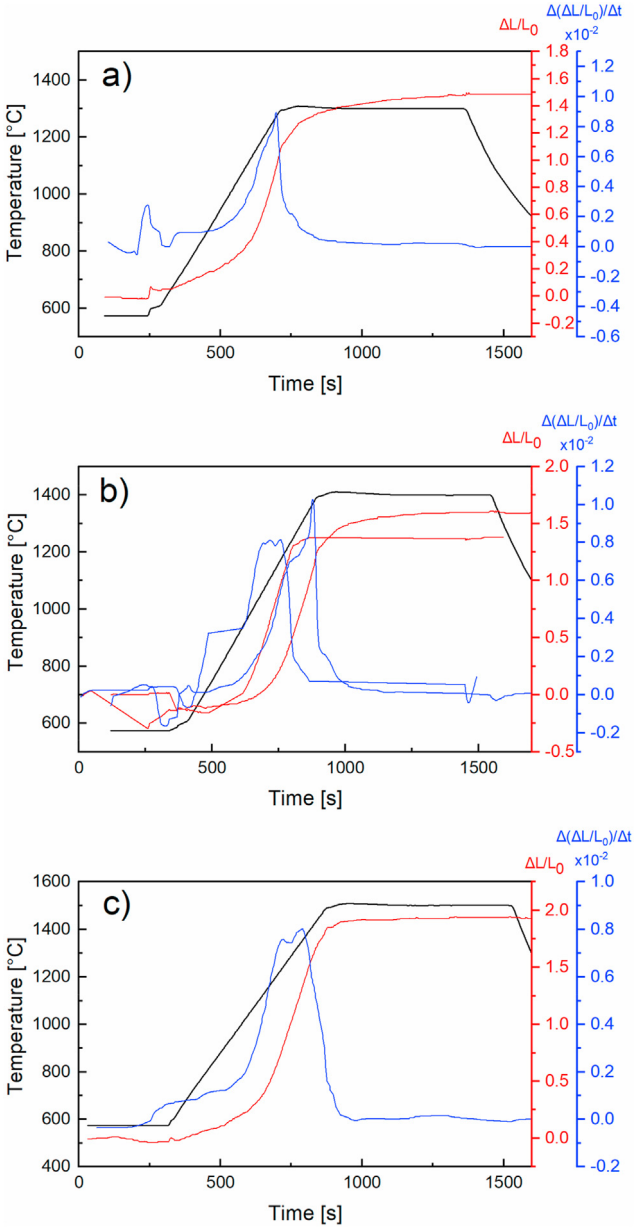

Fig. 2. Relative dimensional change $(\Delta L/L_0)$ for the alumina (20/80) samples and its derivative $\Delta(\Delta L/L_0)/\Delta t$ versus temperature during sintering process with fixed dwell time of 600 s (10 min): a) 1300 °C, 50 MPa; b) 1400 °C, 25–75 MPa; c) 1500 °C, 50 MPa.

of average grain size. The average grain size of produced samples was determined by software processing of microstructure images where the linear intercept technique [38] was applied on ≥250 measurements per sample analysis.

The Vickers hardness (*Hv*) measurements were performed on ceramographically polished (final abrasive size of 3 μm) samples surfaces utilizing a Vickers diamond indenter (Innovatest, Nexus 7500, The Netherlands), applying a load of 10 kg with indentation time of 10 s. The average hardness values were determined by a minimum of 5 repetitions per sample. The dimensions of the corresponding indentations and subsequent crack lengths were processed by an optical microscope (Carl Zeiss, Axio Imager Z1m, Germany). The obtained lengths were also used to determine fracture toughness (K_{Ic}). The Vickers indentation method and proposed formulas have been reported by many researchers [39–41].

Table 2
The validation of SPS optimal conditions.

Optimal conditions			Density, g cm^{-3}	
			20 wt.% of waste content	
Temperature, °C	Dwell time, min	Pressure, MPa	Predicted	Experimental
1450	5	50	3.985	
				3.966
				3.968
				3.965

3. Results and discussion

3.1. Powder characterization

The XRD of starting alumina powders is shown in Fig. 1 exhibiting all characteristic α-alumina (corundum) peaks for both alumina powders. The diffraction reflection patterns of waste and pure alumina powder were matching according to JCPDS - ICDD card no. 46-1212 [42]. The crystalline impurities on the processed XRD patterns of waste alumina powder were not observed. The absence of impurities patterns could be attributed to their low content [43].

The PSD and the cumulative curves of starting alumina powders and their appropriate mixtures are shown in Fig. A.1. The commercial alumina powder (Fig. A.1. a) demonstrated unimodal PSD, compared to the multimodal distribution of waste alumina, with particle size range from 0.20 to 5.12 μm, and average particle size of 0.88 ± 0.54 μm, which is in reasonable agreement with manufacturer specifications. The size range of waste alumina powder was from 0.17 to 214 μm with an average particle size of 3.35 ± 1.03 μm (Fig. A.1. b) which is broader compared to pure alumina powder, as a consequence of the green machining. The PSD for prepared mixtures by ball milling of waste and pure alumina powder are shown in Fig. A.1. c-f). The addition of various amounts of waste alumina powder after ball milling resulted in bimodal PSD for all compositions. Although, an increment of average particle sizes with increasing the waste alumina content was noticed as follows: 20 wt.%-10.87 ± 10.40 μm, 40 wt.%-10.02 ± 10.28 μm, 60 wt.%-4.20 ± 3.12 μm, and 80 wt.%-5.09 ± 3.77 μm. This trend was expected because of the broader PSD of waste alumina powder. The longer time or higher speed rate of ball milling would result in narrower PSD and smaller average size at the expense of higher energy consumption. Hence, the obtained PSD of prepared mixtures represented a compromise between satisfactory powder properties and minimization of energy consumption necessary for milling. The determined specific surface area values were 3.42 m^2/g and 7.57 m^2/g for pure and waste alumina powder, respectively. The crystalline sizes were calculated from XRD diffractograms by the implementation of the Scherrer equation. The obtained crystallite size for pure alumina was 28.9 ± 7.0 nm while for waste alumina powder crystallite size of 24.7 ± 6.2 nm was determined. The difference in crystallite size could contribute to a higher surface area of waste alumina powder [44].

3.2. Sintering conditions

Sintering optimization was conducted on alumina samples, which contained 20 wt.% of waste alumina combined with 80 wt.% of pure alumina powder. Optimal sintering conditions were determined by monitoring the behaviour of alumina samples during the sintering process, with a fixed dwell time of 10 min, while applying sintering temperature (1300 °C–1500 °C) and pressure (25 MPa–75 MPa). The optimization goal was to achieve maximum density of the samples as shown in Fig. 2.

In Fig. 2 a) is shown the impact of the lowest applied sintering temperature of 1300 °C with 50 MPa pressure. The applied sintering temperature was not high enough to obtain full density. The increased

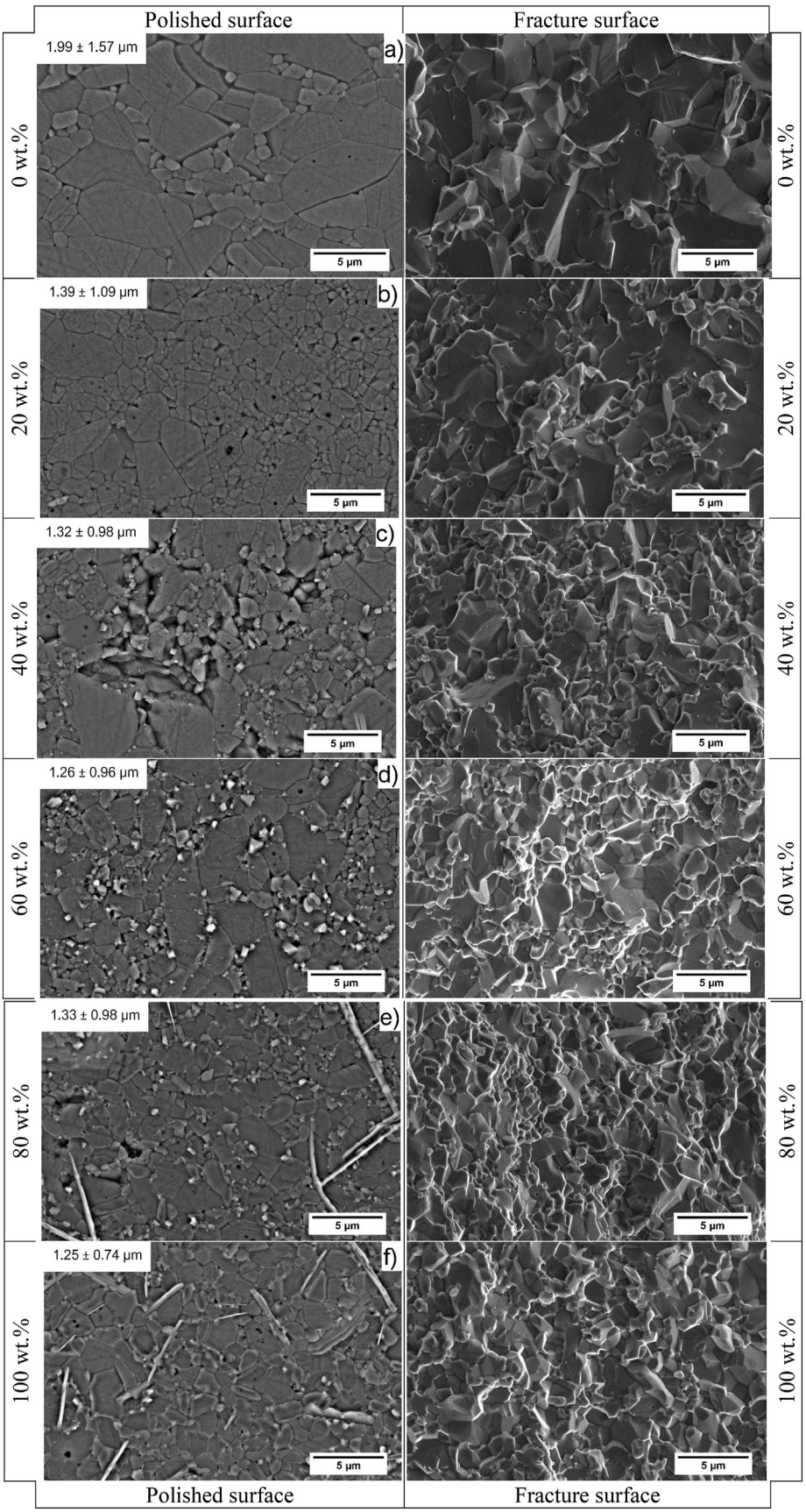

Fig. 3. The SEM images of polished and thermally etched surface at 1400 °C/0.5 h with accompanying fracture surfaces and indicated average grain sizes: a) pure alumina - 1.99 ± 1.57 μm, b) 20 wt.% waste - 1.39 ± 1.09 μm, c) 40 wt.% waste - 1.32 ± 0.98 μm, d) 60 wt.% waste - 1.26 ± 0.96 μm, e) 80 wt.% waste - 1.33 ± 0.98 μm, and f) 100 wt.% waste alumina powder - 1.25 ± 0.74 μm.

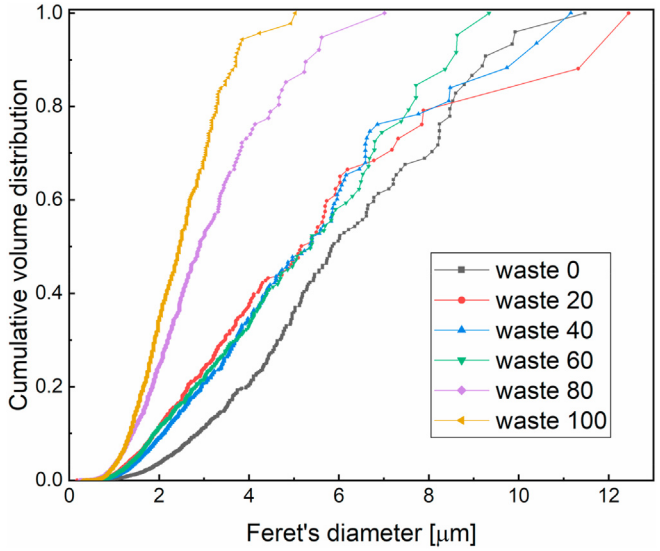

Fig. 4. Cumulative volume grain size distribution versus Feret's diameter of sintered samples with different waste alumina content.

sintering temperature to 1400 °C combined with lower pressure (25 MPa) demonstrated full density at 1375 °C in 881 s while for higher pressure (75 MPa) demonstrated full density at 1250 °C in 709 s as shown in Fig. 2 b). Finally, the impact of the highest sintering temperature (1500 °C) with a moderate pressure of 50 MPa resulted in a full dense sample at 1330 °C in 776 s, which is shown in Fig. 2 c). The investigated sintering conditions confirmed that the full density of alumina samples is achieved around 1400 °C while applying moderate uniaxial pressure of 50 MPa. The optimal values were chosen as follows: 1450 °C sintering temperature, 5 min dwell time, and 50 MPa of uniaxial pressure, with a predicted density value of 3.985 (see Table 2).

Additional figures depicting the obtained densities at optimal SPS conditions versus sample's composition can be found in Fig. B.2 as the effect of applied pressure (50 MPa) on the green density of compacts with varying waste content in Fig. C.3.

3.3. Microstructure characterization

The microstructures of the SPS sintered samples are shown in Fig. 3. The samples were produced at optimal SPS conditions by varying the amounts of waste alumina from 0 to 100 wt.%.

The computed average grain sizes are also indicated in Fig. 3, which demonstrate a slight transition from bigger grain (1.99 ± 1.57 μm) for samples sintered without the addition of waste alumina to smaller grains (1.25 ± 0.74 μm) for samples produced solely from waste alumina powder. The microstructures are relatively fully dense; however, some intergranular pores and mainly elongated spinel grains [45,46] were

Table 3
Reported mechanical properties for alumina samples sintered by SPS.

Source	Sintering conditions	MgO content (wt.%)	Hardness (GPa)	Fracture toughness (MPa $m^{1/2}$)
Pristinskiy et al. [36]	1450 °C, 50 MPa, 3 min	–	16	3.10
		1.00	22	3.15
Shen et al. [34]	1450 °C, 50 MPa, 3 min	–	16.6	3.8
Chakravarty et al. [35]	1150 °C, 50 MPa, 5 min	–	18 ± 1	3.2 ± 0.3
		0.25	20.06 ± 0.5	3.45 ± 0.6

observed with increasing content of waste alumina powder. Also, the abnormal grain growth resulting in slight bimodality with a fraction of bigger grains was present in Fig. 3 a-d) while micrographs in Fig. 3 e, f) demonstrated monomodal grain size distribution. The grain size distribution (GSD) for each composition is depicted in Fig. 4 where a clear distinction between GSD with a higher content of waste alumina compared to smaller content of waste alumina (≤60 wt.%) is visible. From the cumulative volume distribution curves, it was established that 90 vol.% of grains were smaller in diameter than 3.70 μm and 5.26 μm for 100–80 wt.% of waste alumina content. GSD for smaller waste alumina content (≤60 wt.%) demonstrated bigger grains where 90 vol.% of grains were smaller in the diameter range from 8.61 μm to 11.33 μm.

Considering fracture surfaces, the micrographs indicate dominant transgranular failure as a consequence of larger fraction of bigger grains, which is visible on micrographs in Fig. 3 a, b). After increasing the content of waste alumina powder, the intergranular fracture becomes dominant with mainly intergranular crack propagation. In general, the microstructure of pure alumina compared to other micrographs demonstrated a great difference with a clearly visible transition from slightly bigger grain size to evenly distributed grain size microstructure (Fig. 4). The increasing content of the waste alumina in samples resulted in finer and more homogeneous microstructure (bimodal to monomodal) due to the impurities – MgO. Magnesia doping causes reducing the grain boundary mobility of alumina resulting in refinement of microstructure [47,48].

3.4. Mechanical properties

The Vickers hardness (*Hv*10) of alumina with increasing content of waste alumina powder is shown in Fig. 5 a). The substantial increase of hardness from 13.79 ± 1.47 GPa till 19.78 ± 1.27 GPa due to the addition of 20 wt.% waste alumina powder was noticeable, which is in accordance with the presented data in Table 3. The maximal hardness value of 20.81 ± 1.35 GPa was achieved with 80 wt.% of waste alumina content. The increase in hardness could be explained by the refinement of alumina matrix due to sintering additives, i.e. organic binders, MgO, present in waste alumina powder [35]. It should be noted that with the further increase of waste alumina content the change of hardness to higher

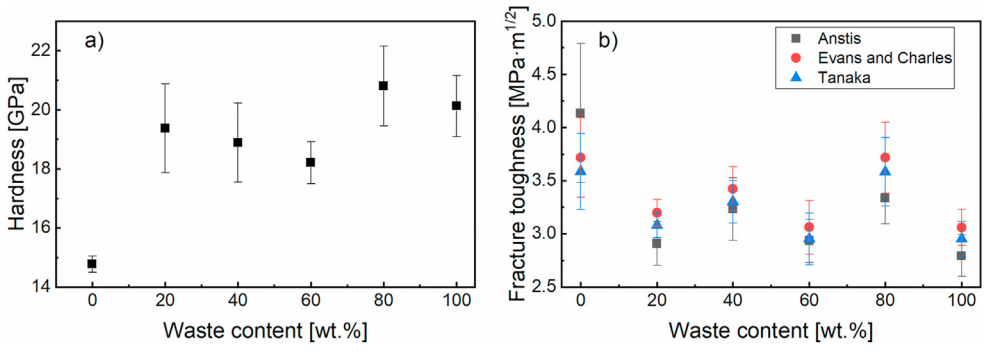

Fig. 5. Effect of waste alumina addition onto a) hardness and b) indentation fracture toughness.

values was obvious.

The fracture toughness of sintered alumina samples was determined by applying the Vickers indentation fracture toughness method. It is worth noting that this method was not used as an exact method for fracture toughness determination but as a mean to assess its trend. The toughness values, which were calculated according to three median models are shown in Fig. 5 b). The pure alumina toughness value is slightly higher compared to the toughness values of samples that contain waste alumina. The samples with the addition of waste alumina tend to level off at a moderate value of 3 MPa $m^{1/2}$, which is in accordance with existing data on advanced alumina ceramics [49]. In general, obtained mechanical properties are in accordance with previously reported studies, related to alumina doping with MgO followed by SPS, as shown in Table 3. Shen et al. [34] systematically examined the influence of SPS conditions on microstructure and mechanical properties. The enhanced mechanical properties were noticed by optimizing SPS conditions to lower sintering temperature where limited grain growth was achieved. Pristinskiy et al. [36] determined a significant increase of hardness by doping alumina with MgO up to 1 wt.% while other properties (flexural strength, fracture toughness) remained unchanged. Chakravarty et al. [35] investigated the effect of magnesia content on the grain size and mechanical properties via SPS. The slight improvements of mechanical properties were noticeable due to the addition of MgO and optimization of SPS conditions. All the above-mentioned studies reported refinement of microstructure and increase of mechanical properties as a consequence of magnesium doping and SPS utilization.

4. Conclusions

This article has thoroughly investigated the possibility of reusing waste alumina powder, which is accumulated during the green machining process. The conducted study strongly suggests the feasibility of using waste alumina powder as secondary raw material where the desired product specifications permit its use. The SPS technique enabled rapid densification of alumina compacts in short times resulting in fine microstructure, which was reflected in higher hardness while fracture toughness remained the same with increasing waste alumina content. The hardness value of 13.79 ± 1.47 GPa was achieved for the pure alumina sample while increasing the waste alumina content resulted in higher hardness values ranging from 18 to 21 GPa. This increase in hardness was attributed to the refinement of alumina matrix due to sintering additives, i.e., MgO, organic binders present in waste alumina powder. In contrast, the fracture toughness demonstrated negligible change with increasing waste alumina content, settling around 3 MPa $m^{1/2}$. The measured values of mechanical properties are in agreement with previously reported values obtained for high purity alumina ceramics doped with MgO while reusing up to 100 wt.% of waste alumina powder as secondary raw material. Recycling the waste alumina scraps enables a significant decrease in primary resource usage, which is a key requirement for the implementation of the circular economy approach in the ceramic manufacturing process.

Declaration of competing interest

The authors declare that they have no known competing financial interests or personal relationships that could have appeared to influence the work reported in this paper.

Acknowledgements

The authors are grateful to the JECS Trust for funding the visit of Milan Vukšić at JSI Ljubljana - Spark plasma sintering of alumina ceramics with addition of waste (secondary) alumina powder (Contract No. 2019232). A. Kocjan acknowledges Slovenian Research Agency funding through research program Ceramics and complementary materials for advanced engineering and biomedical applications (P2-0087). M. Vukšić acknowledges the Croatian Science Foundation - Monolithic and composite advanced ceramics for wear and corrosion protection (Project No. IP–2016-06-6000).

Appendix A. Supplementary data

Supplementary data to this article can be found online at https://doi.org/10.1016/j.oceram.2021.100076.

References

[1] G. Moraga, S. Huysveld, F. Mathieux, G.A. Blengini, L. Alaerts, K. Van Acker, S. de Meester, J. Dewulf, Circular economy indicators: what do they measure? Resour. Conserv. Recycl. 146 (2019) 452–461, https://doi.org/10.1016/j.resconrec.2019.03.045.
[2] M. Lieder, A. Rashid, Towards circular economy implementation: a comprehensive review in context of manufacturing industry, J. Clean. Prod. 115 (2016) 36–51, https://doi.org/10.1016/j.jclepro.2015.12.042.
[3] P. Morseletto, Targets for a circular economy, Resour. Conserv. Recycl. 153 (2020), 104553, https://doi.org/10.1016/j.resconrec.2019.104553.
[4] Towards a Circular Economy: Business Rationale for an Accelerated Transition, 2015.
[5] S.S. Hossain, P.K. Roy, Sustainable ceramics derived from solid wastes: a review, J. Asian Ceram. Soc. 8 (4) (2020) 984–1009, https://doi.org/10.1080/21870764.2020.1815348.
[6] A New Circular Economy Action Plan: For a Cleaner and More Competitive Europe, 2020. Available online: https://eur-lex.europa.eu/legal-content/EN/TXT/?qid=1583933814386&uri=COM:2020:98:FIN.
[7] G.L.F. Benachio, M.d.C.D. Freitas, S.F. Tavares, Circular economy in the construction industry: a systematic literature review, J. Clean. Prod. 260 (2020), 121046, https://doi.org/10.1016/j.jclepro.2020.121046.
[8] Y. Tian, S.E. Demirel, M.M.F. Hasan, E.N. Pistikopoulos, An overview of process systems engineering approaches for process intensification: state of the art, Chem. Eng. Process. Process Intens. 133 (2018) 160–210, https://doi.org/10.1016/j.cep.2018.07.014.
[9] F. Jia, S. Yin, L. Chen, X. Chen, The circular economy in the textile and apparel industry: a systematic literature review, J. Clean. Prod. 259 (2020), 120728, https://doi.org/10.1016/j.jclepro.2020.120728.
[10] S. Ke, Y. Wang, Z. Pan, C. Ning, S. Zheng, Recycling of polished tile waste as a main raw material in porcelain tiles, J. Clean. Prod. 115 (2016) 238–244, https://doi.org/10.1016/j.jclepro.2015.12.064.
[11] B. Tarhan, M. Tarhan, T. Aydin, Reusing sanitaryware waste products in glazed porcelain tile production, Ceram. Int. 43 (3) (2017) 3107–3112, https://doi.org/10.1016/j.ceramint.2016.11.123.
[12] P.F. Gouveia, L.M. Schabbach, J.C.M. Souza, B. Henriques, J.A. Labrincha, F.S. Silva, M.C. Fredel, J. Mesquita-Guimarães, New perspectives for recycling dental zirconia waste resulting from CAD/CAM manufacturing process, J. Clean. Prod. 152 (2017) 454–463, https://doi.org/10.1016/j.jclepro.2017.03.117.
[13] H. Ding, J.K.-H. Tsoi, C.-w. Kan, J.P. Matinlinna, A simple solution to recycle and reuse dental CAD/CAM zirconia block from its waste residuals, J. Prosthodont. Res. advpub (2021), https://doi.org/10.2186/jpr.JPR_D_20_00002.
[14] J. Tao, Z. Chen, S. Yu, Z. Liu, Integration of life cycle assessment with computer-aided product development by a feature-based approach, J. Clean. Prod. 143 (2017) 1144–1164, https://doi.org/10.1016/j.jclepro.2016.12.005.
[15] D. Pravarthana, D. Chateigner, L. Lutterotti, M. Lacotte, S. Marinel, P.A. Dubos, I. Hervas, E. Hug, P.A. Salvador, W. Prellier, Growth and texture of spark plasma sintered Al2O3 ceramics: a combined analysis of X-rays and electron back scatter diffraction, J. Appl. Phys. 113 (15) (2013) 153510, https://doi.org/10.1063/1.4802439.
[16] M. López-Alonso, M.J. Martinez-Echevarria, L. Garach, A. Galán, J. Ordoñez, F. Agrela, Feasible use of recycled alumina combined with recycled aggregates in road construction, Construct. Build. Mater. 195 (2019) 249–257, https://doi.org/10.1016/j.conbuildmat.2018.11.084.
[17] G. Sua-iam, N. Makul, Use of recycled alumina as fine aggregate replacement in self-compacting concrete, Construct. Build. Mater. 47 (2013) 701–710, https://doi.org/10.1016/j.conbuildmat.2013.05.065.
[18] G. Sua-iam, N. Makul, Incorporation of high-volume fly ash waste and high-volume recycled alumina waste in the production of self-consolidating concrete, J. Clean. Prod. 159 (2017) 194–206, https://doi.org/10.1016/j.jclepro.2017.05.075.
[19] M. Vukšić, I. Žmak, L. Ćurković, D. Ćorić, P. Jenuš, A. Kocjan, Evaluating recycling potential of waste alumina powder for ceramics production using response surface methodology, J. Mater. Res. Technol. 11 (2021) 866–874, https://doi.org/10.1016/j.jmrt.2021.01.064.
[20] M. Vukšić, I. Žmak, L. Ćurković, D. Ćorić, Effect of additives on stability of alumina—waste alumina suspension for slip casting: optimization using Box-Behnken design, Materials 12 (11) (2019), https://doi.org/10.3390/ma12111738.
[21] M. Vukšić, M. Ljubek, I. Žmak, L. Ćurković, Hybrid microwave sintering of alumina ceramics which contain waste alumina, Nanomater. Sci. Eng. 4 (2) (2020) 8, https://doi.org/10.34624/nmse.v2i4.21069.
[22] The European Commission's BREF document on the Ceramic Manufacturing Industry (CER), Available online: https://eippcb.jrc.ec.europa.eu/sites/default/files/2019-11/cer_bref_0807.pdf (accessed 04.02.20).

[23] K. Rajeswari, U.S. Hareesh, R. Subasri, D. Chakravarty, R. Johnson, Comparative evaluation of spark plasma (SPS), microwave (MWS), two stage sintering (TSS) and conventional sintering (CRH) on the densification and micro structural evolution of fully stabilized zirconia ceramics, Sci. Sinter. 42 (2010), https://doi.org/10.2298/SOS1003259R.
[24] E. Töldsepp, F. Schoenstein, M. Amamra, R. Saar, E. Feldbach, A. Kanaev, M. Kirm, Spark plasma sintering of ultra-porous γ-Al2O3, Ceram. Int. 42 (10) (2016) 11709–11715, https://doi.org/10.1016/j.ceramint.2016.04.089.
[25] G.C. Wei, A. Hecker, D.A. Goodman, Translucent polycrystalline alumina with improved resistance to sodium attack, J. Am. Ceram. Soc. 84 (12) (2001) 2853–2862, https://doi.org/10.1111/j.1151-2916.2001.tb01105.x.
[26] D. Tiwari, B. Basu, K. Biswas, Simulation of thermal and electric field evolution during spark plasma sintering, Ceram. Int. 35 (2) (2009) 699–708, https://doi.org/10.1016/j.ceramint.2008.02.013.
[27] Q. Tian, J. Dai, L. Xu, X. Wang, Advance of sintering methods of high purity alumina ceramics, Key Eng. Mater. 703 (2016) 76–80. https://doi.org/10.4028/www.scientific.net/KEM.703.76.
[28] S.-X. Song, Z. Wang, G.-P. Shi, Heating mechanism of spark plasma sintering, Ceram. Int. 39 (2013) 1393–1396, https://doi.org/10.1016/j.ceramint.2012.07.080.
[29] R. Chaim, On densification mechanisms of ceramic particles during spark plasma sintering, Scripta Mater. 115 (2016) 84–86, https://doi.org/10.1016/j.scriptamat.2016.01.010.
[30] C. Liu, M. Xiang, Z. Fu, Z. Shen, Y. Xiong, Microstructural refinement in spark plasma sintering 3Y-TZP nanoceramics, J. Eur. Ceram. Soc. 36 (10) (2016) 2565–2571, https://doi.org/10.1016/j.jeurceramsoc.2016.03.019.
[31] M. Demuynck, J.-P. Erauw, O. Van der Biest, F. Delannay, F. Cambier, Densification of alumina by SPS and HP: a comparative study, J. Eur. Ceram. Soc. 32 (9) (2012) 1957–1964, https://doi.org/10.1016/j.jeurceramsoc.2011.10.031.
[32] J.G. Santanach, A. Weibel, C. Estournès, Q. Yang, C. Laurent, A. Peigney, Spark plasma sintering of alumina: study of parameters, formal sintering analysis and hypotheses on the mechanism(s) involved in densification and grain growth, Acta Mater. 59 (4) (2011) 1400–1408, https://doi.org/10.1016/j.actamat.2010.11.002.
[33] K.T. Lee, S.I. Cha, K.T. Kim, K.H. Lee, S.H. Hong, Sintering behavior, microstructural evolution, and mechanical properties of ultra-fine grained alumina synthesized via in-situ spark plasma sintering, Ceram. Int. 42 (3) (2016) 4290–4297, https://doi.org/10.1016/j.ceramint.2015.11.106.
[34] Z. Shen, M. Johnsson, Z. Zhao, M. Nygren, Spark plasma sintering of alumina, J. Am. Ceram. Soc. 85 (8) (2002) 1921–1927, https://doi.org/10.1111/j.1151-2916.2002.tb00381.x.
[35] D. Chakravarty, S. Bysakh, K. Muraleedharan, T.N. Rao, R. Sundaresan, Spark plasma sintering of magnesia-doped alumina with high hardness and fracture toughness, J. Am. Ceram. Soc. 91 (1) (2008) 203–208, https://doi.org/10.1111/j.1551-2916.2007.02094.x.
[36] Y. Pristinskiy, N. Washington Solis Pinargote, A. Smirnov, The effect of MgO addition on the microstructure and mechanical properties of alumina ceramic obtained by spark plasma sintering, Mater. Today Proc. 19 (2019) 1990–1993, https://doi.org/10.1016/j.matpr.2019.07.058.
[37] E. Yalamaç, A. Trapani, S. Akkurt, Sintering and microstructural investigation of gamma–alpha alumina powders, Eng. Sci. Technol. Int. J. 17 (1) (2014) 2–7, https://doi.org/10.1016/j.jestch.2014.02.001.
[38] M.I. Mendelson, Average grain size in polycrystalline ceramics, J. Am. Ceram. Soc. 52 (8) (1969) 443–446, https://doi.org/10.1111/j.1151-2916.1969.tb11975.x.
[39] Y. Feng, T. Zhang, Determination of fracture toughness of brittle materials by indentation, Acta Mech. Solida Sin. 28 (3) (2015) 221–234, https://doi.org/10.1016/S0894-9166(15)30010-0.
[40] A. Nastic, A. Merati, M. Bielawski, M. Bolduc, O. Fakolujo, M. Nganbe, Instrumented and Vickers indentation for the characterization of stiffness, hardness and toughness of zirconia toughened Al2O3 and SiC armor, J. Mater. Sci. Technol. 31 (8) (2015) 773–783, https://doi.org/10.1016/j.jmst.2015.06.005.
[41] K. Tanaka, Elastic/plastic indentation hardness and indentation fracture toughness: the inclusion core model, J. Mater. Sci. 22 (4) (1987) 1501–1508, https://doi.org/10.1007/BF01233154.
[42] F. Feret, D. Roy, C. Boulanger, Determination of alpha and beta alumina in ceramic alumina by X-ray diffraction, Spectrochim. Acta B Atom Spectrosc. 55 (2000) 1051–1061, https://doi.org/10.1016/S0584-8547(00)00225-1.
[43] B.A. Latella, B.H. O'Connor, Detection of minor crystalline phases in alumina ceramics using synchrotron radiation diffraction, J. Am. Ceram. Soc. 80 (11) (1997) 2941–2944, https://doi.org/10.1111/j.1151-2916.1997.tb03216.x.
[44] C. Bueno-Ferrer, S. Parres-Esclapez, D. Lozano-Castelló, A. Bueno-López, Relationship between surface area and crystal size of pure and doped cerium oxides, J. Rare Earths 28 (5) (2010) 647–653, https://doi.org/10.1016/S1002-0721(09)60172-1.
[45] M. Michálková, M. Michálek, G. Blugan, J. Kuebler, The influence of spinel and magnesia powder bed on mechanical properties of alumina sintered under air and nitrogen atmosphere, Adv. Appl. Ceram. 117 (8) (2018) 485–492, https://doi.org/10.1080/17436753.2018.1502063.
[46] I. Ganesh, A review on magnesium aluminate (MgAl2O4) spinel: synthesis, processing and applications, Int. Mater. Rev. 58 (2) (2013) 63–112, https://doi.org/10.1179/1743280412Y.0000000001.
[47] S.J. Bennison, M.P. Harmer, Effect of magnesia solute on surface diffusion in sapphire and the role-of magnesia in the sintering of alumina, J. Am. Ceram. Soc. 73 (4) (1990) 833–837, https://doi.org/10.1111/j.1151-2916.1990.tb05122.x.
[48] S.J. Dillon, M. Tang, W.C. Carter, M.P. Harmer, Complexion: a new concept for kinetic engineering in materials science, Acta Mater. 55 (18) (2007) 6208–6218, https://doi.org/10.1016/j.actamat.2007.07.029.
[49] P. Auerkari, Mechanical and Physical Properties of Engineering Alumina Ceramics, Julkaisija-Utgivare, VTT Offsetpaino, Espoo, 1996.